J. Fluid Mech. (1976), *vol.* 73, *part* 1, *pp.* 165–188
Printed in Great Britain

Experimental investigation of turbulent shear flow with quadratic mean-velocity profiles

By H. K. RICHARDS AND J. B. MORTON

Department of Engineering Science and Systems, University of Virginia, Charlottesville

(Received 12 April 1975)

Three turbulent shear flows with quadratic mean-velocity profiles are generated by using an appropriately designed honeycomb and parallel-rod grids with adjustable rod spacing. The details of two of the flow fields, with quadratic mean-velocity profiles with constant positive mean-shear gradients ($\partial^2\overline{U}_1/\partial X_2^2 > 0$), are obtained, and include, in the mean flow direction, the development and distribution of mean velocities, fluctuating velocities, Reynolds stresses, microscales, integral scales, energy spectra, shear correlation coefficients and two-point spatial velocity correlation coefficients. A third flow field is generated with a quadratic mean velocity profile with constant negative mean-shear gradient ($\partial^2\overline{U}_1/\partial X_2^2 < 0$), to investigate in the mean flow direction the effect of the change in sign on the resulting field. An open-return wind tunnel with a $2 \times 2 \times 20$ ft test-section is used.

1. Introduction

Experimental determination of the development of turbulence in a shear flow with a quadratic mean-velocity profile is the purpose of this investigation.†

Corrsin (1957) pointed out that fully-developed turbulent shear flows (boundary-layer, jet, wake) have their turbulent shear stress carried by eddies comparable in size to the lateral extent of the flow boundaries. Hence, the flow may be affected by the boundary conditions. This led him to suggest experimental studies of a turbulent shear flow in which the complicating effects of the boundaries are absent. The simplest possible shear flow meeting this requirement is a homogeneous turbulent one, maintained by a uniform mean shear.

The first attempt at generating this type of flow was made by Rose (1966), using a non-uniformly spaced, parallel-rod grid as a flow generator. The main departures from homogeneity in the resulting flow field were in the longitudinal and lateral distributions of the turbulent scales. Champagne, Harris & Corrsin (1970) eliminated the lateral inhomogeneity of the turbulent scales, by using a transverse array of channels of equal widths but varying resistances as a flow generator. Rose (1970) and Hwang (1971) investigated the effect of initial conditions in a linear mean-shear flow, by using various combinations of a parallel-rod

† This paper is based on a Ph.D. dissertation by one of the authors (H.K.R.). For details, refer to Richards (1971).

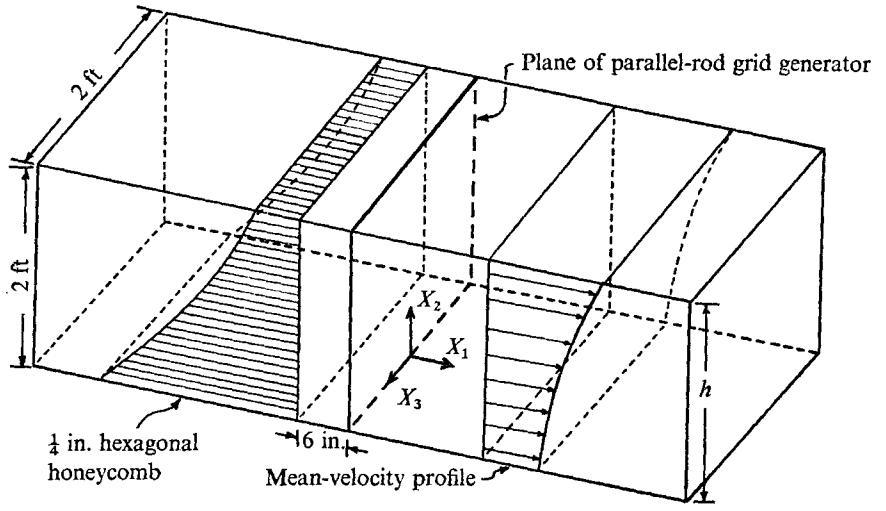

FIGURE 1. Flow-generation system.

Co-ordinate	Mean-velocity component	R.m.s. fluctuating velocity component
X_1	$\bar{U}_1 = U(X_2)$	u_1'
X_2	$\bar{U}_2 = 0$	u_2'
X_3	$\bar{U}_3 = 0$	u_3'

grid with uniform spacing, a honeycomb and grids of different geometries. Harris, Graham & Corrsin (unpublished manuscript) looked at the effect of more intense shear, and established the downstream development of the turbulence in linear mean shear flows for strain rates up to $40\,s^{-1}$ and total strains of about 10.

The purpose of the present study is to generate a flow with a quadratic mean-velocity profile, and to observe the effect of the gradient of the mean shear on the resulting turbulence.

2. Description of apparatus and facilities

2.1. *The test facility*

The test facility is the same as that used by Rose (1970). It will not be described further.

2.2. *The mean-shear-flow generators*

The desired flow in this experiment is one with a quadratic mean-velocity profile. The flow (figure 1) passes through a ¼ in. cell-diameter hexagonal honeycomb of suitable design, which by itself generates a linear mean-velocity profile. 6 in. downstream from the exit plane of the honeycomb, a parallel round-rod grid with non-uniform spacing is placed, which provides the quadratic mean-velocity profile. Two different grid generators are used. Both are composed of aluminum rods, one of $\frac{3}{8}$ in. dia. the other $\frac{3}{16}$ in. For details, see Richards (1971).

The parallel-rod grid was placed downstream from the honeycomb section because the effect of this section on the flow was so great that it was difficult to place the grid in front of it and achieve the desired results.

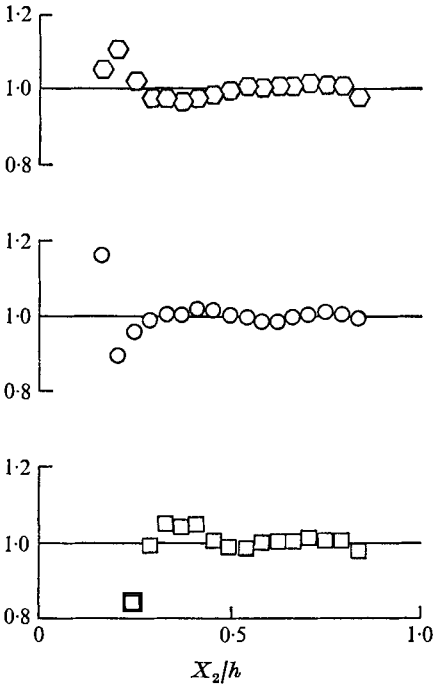

FIGURE 2. $(\overline{U}_1(X_2) - A - BX_2)/CX_2^2$ against X_2/h, where A, B, C are least-squares best-fit coefficients for a quadratic profile. ⬡, $\partial^2 U_1/\partial X_2^2 > 0$, $\frac{3}{16}$ rods; ○, $\partial^2 \overline{U}_1/\partial X_2^2 > 0$, $\frac{3}{8}$ rods; □, $\partial^2 \overline{U}_1/\partial X_2^2 < 0$.

There are four possible forms for the quadratic velocity profile. These are $\partial \overline{U}_1/\partial X_2 > 0$ or < 0 and $\partial^2 \overline{U}_1/\partial X_2^2 > 0$ or < 0. Only two of these cases are measured here: those with $\partial \overline{U}_1/\partial X_2 > 0$. The other two flows are exactly the same under the co-ordinate transformation $X_2 \rightarrow -X_2$. Thus, the two flows with $\partial \overline{U}_1/\partial X_2 < 0$ are the same as the flows with $\partial \overline{U}_1/\partial X_2 > 0$, except that they are viewed 'upside-down'.

The hexagonal honeycomb used upstream of the parallel-rod generators was damaged slightly on its upstream face just before this investigation. The results presented here, and information from an investigation by Hwang (1971), show no appreciable influence on the downstream flow, so the damage is considered minor.

For the first two profiles tested, the grids were designed such that the gradient of the mean velocity $\partial \overline{U}_1/\partial X_2 > 0$, and the gradient of the mean-shear $\partial^2 \overline{U}_1/\partial X_2^2$ was a positive constant. The reason for this design is to make the total strain $(X_1/U_1)(\partial \overline{U}_1/\partial X_2)$ to which the turbulence is subjected relatively constant laterally at any X_1 position. This point concerning the importance of the role of total strain is discussed further in § 3.

An additional field was generated, one with quadratic mean velocity profile such that $\partial \overline{U}_1/\partial X_2 > 0$ and $\partial^2 \overline{U}_1/\partial X_2^2$ was a negative constant. This was generated using the $\frac{3}{8}$ rod grid.

The resulting mean-velocity profiles were within 0·5% of a quadratic profile based on a least-squares fit to the data. Figure 2 illustrates the error in the

Nominal $\partial^2\overline{U}_1/\partial X_2^2$	A	B	C
12·3	40·5724	3·328	6·13
8·4	38·679	7·138	4·18
−6·7	31·27	22·1	−3·37

TABLE 1. Coefficients of the least-squares fit to the mean velocity in the form $\overline{U}_1(X_2) = A + BX_2 + CX_2^2$

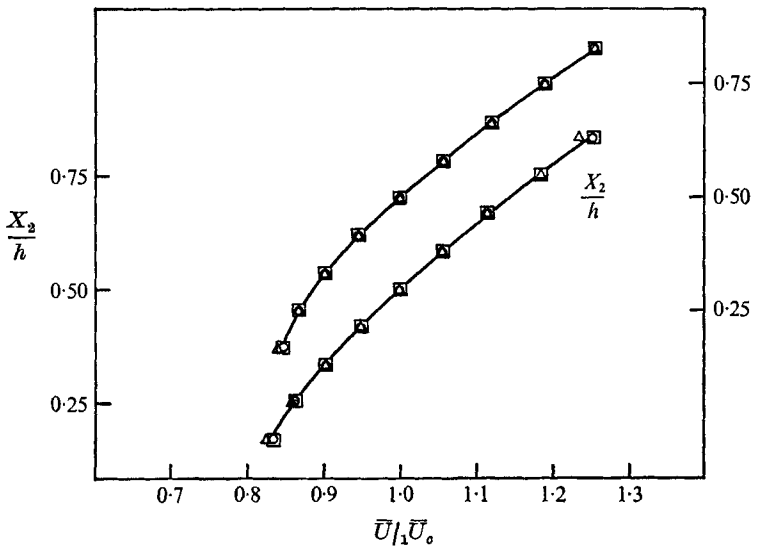

FIGURE 3. Longitudinal development of mean velocity. Upper curve and right axis, $\frac{3}{16}$ rods; lower curve and left axis, $\frac{3}{8}$ rods. X_1/h: □, 5; ○, 7; △, 9.

curvature for the three profiles. The values of A, B and C, the coefficients of the fitted quadratic profile, are given in table 1.

Figure 2 shows that, over the range $0{\cdot}25 \leqslant X_2/h \leqslant 0{\cdot}8$, the curvature is very nearly constant. This corresponds to approximately 1·1 ft.

3. Results

3.1. *Form and development of mean-velocity fields*

The two profiles that have a constant positive mean-shear gradient are each quadratic to within 0·3 % of a least-squares fit. The mean shear $\partial\overline{U}_1/\partial X_2$ at the tunnel centre-line is about 15·6 s^{-1} in both cases. The gradient of the mean shear $\partial^2\overline{U}_1/\partial X_2^2$ is 8·4 $(ft\,s)^{-1}$ in the case of the $\frac{3}{8}$ rod generator, and 12·3 $(ft\,s)^{-1}$ in that of the $\frac{3}{16}$ rod. A comparison of the mean shear at several X_2/h locations is given in table 2. The centre-line velocity $\overline{U}_c$ is 50 ft s^{-1} in all runs. It is clear from figure 3 that the mean-velocity fields maintain essentially the same distribution throughout the length of the test section. The effects of the boundary layer appear at a distance from the walls of $X_2/h \simeq 0{\cdot}2$ at a longitudinal position of $X_1/h = 9{\cdot}0$.

X_2/h	$\frac{3}{8}$ rods	$\frac{3}{16}$ rods
0·25	11·3	9·5
0·33	12·7	11·5
0·41	14·1	13·6
0·50	15·6	15·6
0·59	16·9	17·6
0·67	18·3	19·6
0·75	19·7	21·7
$\frac{d^2\overline{U}_1}{dX_2^2}$ (ft s)$^{-1}$	8·4	12·3

TABLE 2. Mean shear $d\overline{U}_1/dX_2$ s^{-1} lateral distributions. $X_1/h = 5{\cdot}0$.

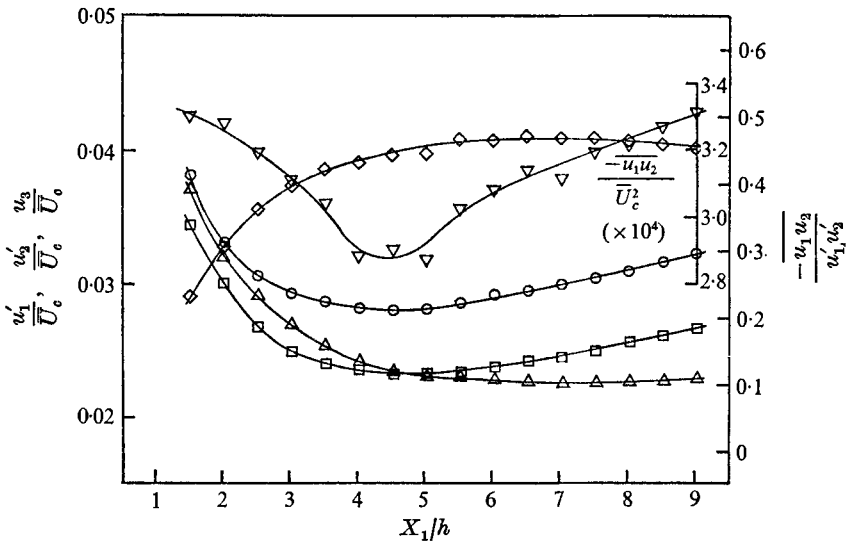

FIGURE 4. Longitudinal development of turbulence with mean-velocity profile $\partial^2\overline{U}_1/\partial X_2^2 = 8{\cdot}4$ (ft s)$^{-1}$, $X_2/h = 0{\cdot}50$, $X_2/h = -0{\cdot}07$. $\frac{3}{8}$ rods. ○, $u_1'/\overline{U}_c$; △, $u_2'/\overline{U}_c$; □, u_3'/U_c. ◇, $\overline{u_1u_2}/u_1'u_2'$; ▽, $\overline{u_1u_2}/\overline{U}_c^2$.

The quadratic mean-velocity field with $\partial^2\overline{U}_1/\partial X_2^2 < 0$ also maintains its distributions throughout the length of the test section. The value of the second derivative of the velocity $\partial^2\overline{U}_1/\partial X_2^2$ for this flow is $-6{\cdot}7$ (ft s)$^{-1}$. The mean shear at the centre-line of the wind tunnel is $15{\cdot}4\,\text{s}^{-1}$.

3.2. *Centre-line development of the fluctuating velocity fields*

The downstream development of the intensities of the fluctuating velocity components and the values of the shear correlation coefficients for the quadratic velocity profiles ($\partial^2\overline{U}_1/\partial X_2^2 > 0$) generated by the $\frac{3}{8}$ and $\frac{3}{16}$ rod grids are presented in figures 4 and 5. The turbulent intensities decay from the large values just downstream of the generators to minimum values, then increase monotonically. The u_1' and u_3' components reach minimum values near $X_1/h = 5{\cdot}0$, while the u_2' component reaches a minimum at about $X_1/h = 7{\cdot}5$.

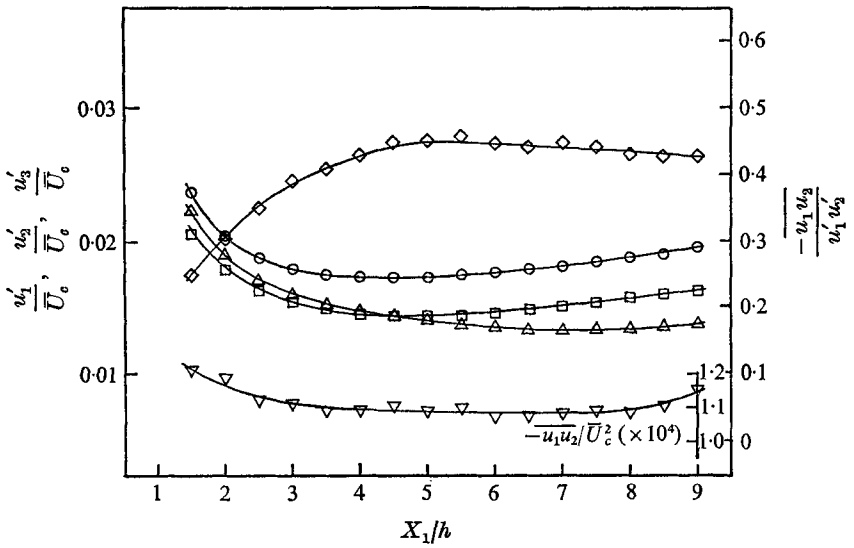

FIGURE 5. Longitudinal development of turbulence with mean-velocity profile $\partial^2\overline{U}_1/\partial X_2^2 = 12{\cdot}3$ (ft s)$^{-1}$, $X_2/h = 0{\cdot}50$, $X_3/h = -0{\cdot}07$. $\frac{3}{16}$ rods. Symbol key as for figure 4.

In both experimental flows, the u_2' fluctuating component is larger than u_3' just downstream of the grid generators, but at the exit plane of the test section this is reversed. The intensity of the two components is equal at

$$X_1/h \simeq 4{\cdot}5 \quad ((X_1/\overline{U}_1)(\partial\overline{U}_1/\partial X_2) \simeq 2{\cdot}9).$$

This is analogous to the findings of Champagne *et al.* (1970) and Hwang (1971) in their investigations with linear mean-velocity shear flows. In both their cases, the intensities of the two components were equal at

$$X_1/h \simeq 6{\cdot}5 \quad ((X_1/\overline{U}_1)(\partial\overline{U}_1/\partial X_2) \simeq 2{\cdot}1).$$

The longitudinal development of the u_1' component is very similar to that of u_3'. Both reach a minimum value at essentially the same downstream position, and increase to about 15% above their minimum values at the exit plane. The u_2' intensity also increases downstream of $X_1/h = 7{\cdot}5$, but by only about 2–4%. The shear correlation coefficients reach a maximum value of about 0·46 in the vicinity of $X_1/h = 5{\cdot}0$, then decrease slightly in the remainder of the test section. The value of 0·46 is comparable to those observed in previous investigations of 'nearly' homogeneous shear flows. (Rose 1966; Champagne *et al.* 1970; Hwang 1971.) The rather peculiar behaviour of the shear covariance function $\overline{u_1u_2}/\overline{U}_c^2$ in figure 4, as compared with figure 5, appears to be caused by the greater slopes in the $u_1'/\overline{U}_c$ and $u_2'/\overline{U}_c$ decay curves. However, the correlation coefficient $\overline{u_1u_2}/u_1'u_2'$ is consistent with other data. The longitudinal development of the fluctuating components of the additional flow field generated with the $\frac{3}{8}$ rod grid is presented in figure 6. The behaviour of the component intensity decay and growth is essentially the same as for the earlier two cases, where the velocity profiles have constant positive mean-shear gradients.

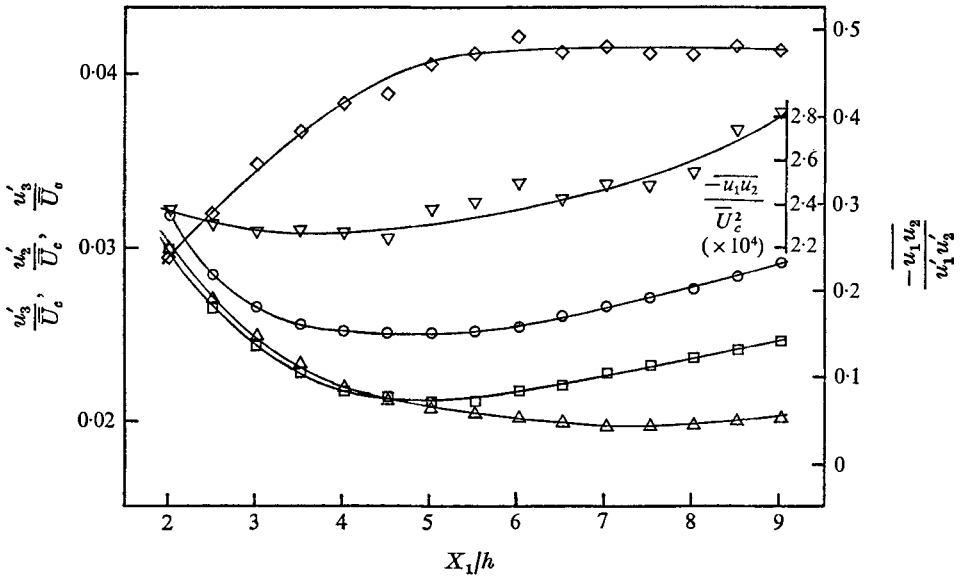

FIGURE 6. Longitudinal development of turbulence with mean-velocity profile $\partial^2\overline{U}_1/\partial X_2^2 = -6{\cdot}7$ (ft s)$^{-1}$, $X_2/h = 0{\cdot}50$, $X_3/h = -0{\cdot}07$. $\frac{3}{8}$ rods. Symbol key as for figure 4.

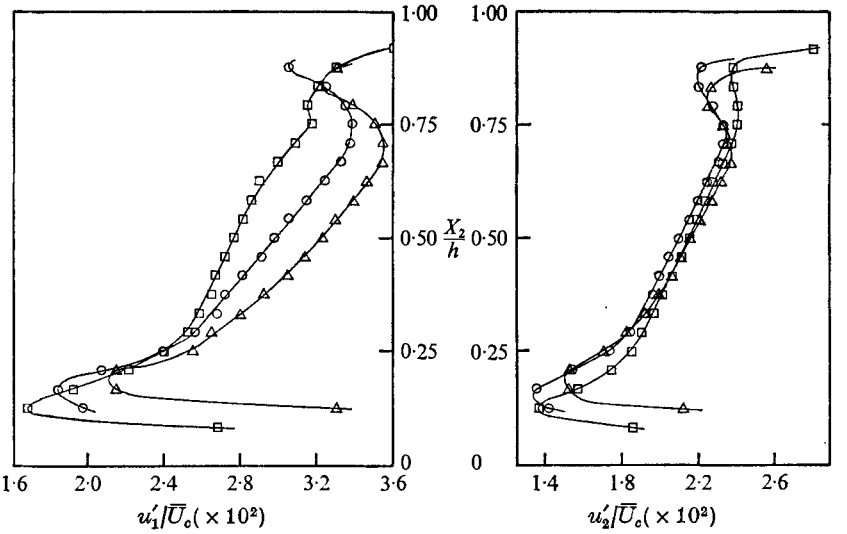

FIGURE 7. Lateral surveys of turbulence with mean-velocity profile $\partial^2\overline{U}_1/\partial X_2^2 = 8{\cdot}4$ (ft s)$^{-1}$, $X_3/h = -0{\cdot}07$. $\frac{3}{8}$ rods. Symbol key as for figure 3.

3.3. *Lateral surveys of the fluctuating velocity fields*

Lateral surveys of various quantities associated with the fluctuating velocity fields were made at three longitudinal positions, viz.

$$X_1/h = 5{\cdot}0, \quad X_1/h = 7{\cdot}0 \quad \text{and} \quad X_1/h = 9{\cdot}0.$$

Preliminary investigations had shown $X_1/h = 5{\cdot}0$ to be the point of minimum

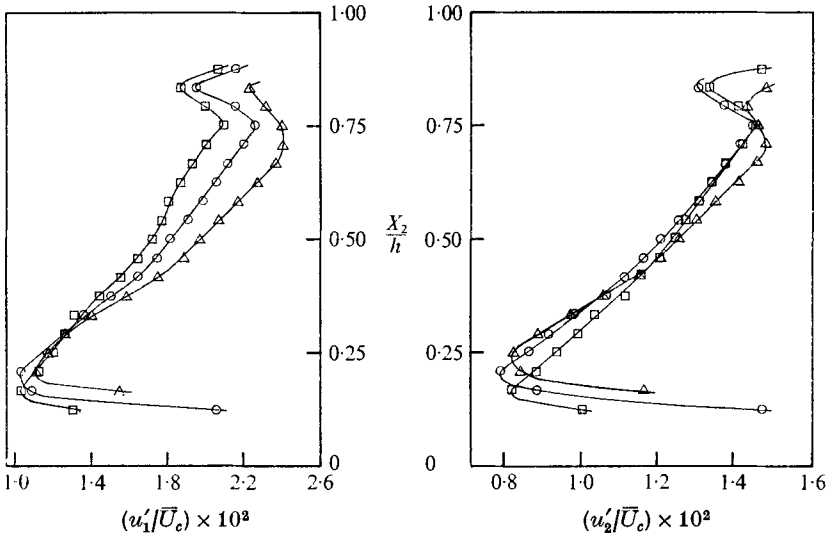

FIGURE 8. Lateral surveys of turbulence with mean-velocity profile $\partial^2\overline{U}_1/\partial X_2^2 = 12{\cdot}3$ (ft s)$^{-1}$, $X_3/h = -0{\cdot}07$. $\frac{3}{16}$ rods. Symbol key as for figure 3.

intensity of the u_1' component, and that the lateral distributions of turbulence quantities were quite smooth. The limit $X_1/h = 9{\cdot}0$ was fixed by the length of the wind tunnel. Figures 7 and 8 depict the lateral distributions of the u_1' and u_2' intensities for the flow fields with constant positive mean-shear gradients.

In both flow fields, the principal characteristics shown by the u_1' component are an essentially linear variation in the X_2 direction at a given longitudinal position, and an increase in the gradient $\partial u_1'/\partial X_2$ in the downstream direction. The increase in the gradient $\partial u_1'/\partial X_2$ is the significant result. This is due to the variation of the total strain $(X_1/\overline{U}_1)(\partial\overline{U}_1/\partial X_2)$ in the X_2 direction. The importance of this parameter will be discussed in later sections.

The lateral surveys of the u_2' component shown in figures 7 and 8 are not as definitive, since the u_2' component reaches its minimum value at values of X_1/h between 5 and 9. The intensity of the u_2' component also varies almost linearly at a given X_1/h position and the gradient $\partial u_2'/\partial X_2$ increases in the X_1 direction. This phenomenon is related to the total strain to which the turbulence has been subjected. As in the case of the u_1' intensity, the parameter $(X_1/\overline{U}_1)(\partial\overline{U}_1/\partial X_2)$ is the important quantity in predicting the downstream development of the u_2' component. It is found that the u_1' intensities reach minimum values in these flows at total strains of about 3·0, while u_2' intensities reach them at total strains of about 4·5. This difference is due to the two-dimensional nature of the mean flow, and the way the turbulent energy is partitioned among the components (Richards 1971).

Figure 8 shows a slight change in the slope of the u_1' and u_2' curves at $X_2/h = 0{\cdot}45$. The cause must be associated with the small departures from a quadratic of the mean-velocity profile, as seen in figure 2. A least-squares fit of the mean-velocity data points between $X_2/h = 0{\cdot}25$ and 0·75 shows a maximum difference of 0·1 % between calculated and experimental values. This gives some

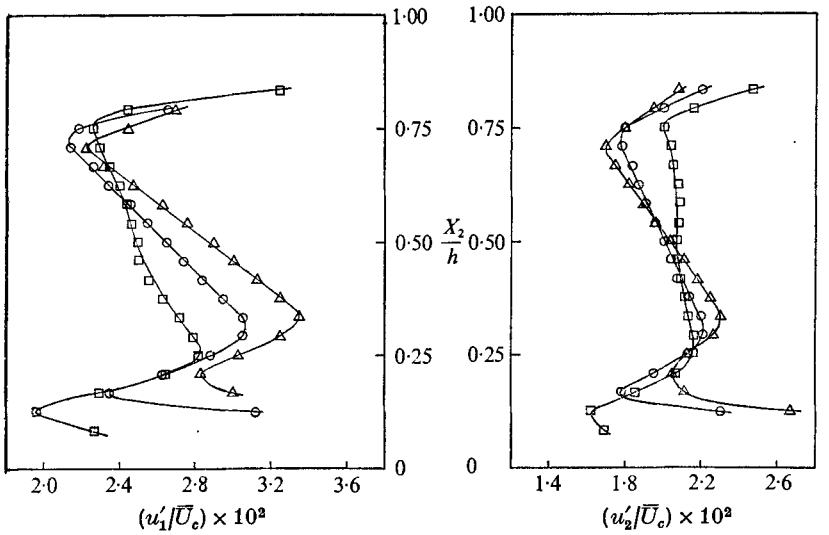

FIGURE 9. Lateral surveys of turbulence with mean-velocity profile $\partial^2\overline{U}_1/\partial X_2^2 = -6{\cdot}7\,(\text{ft s})^{-1}$, $X_3/h = -0{\cdot}07$. $\frac{3}{8}$ rods. Symbol key as for figure 3.

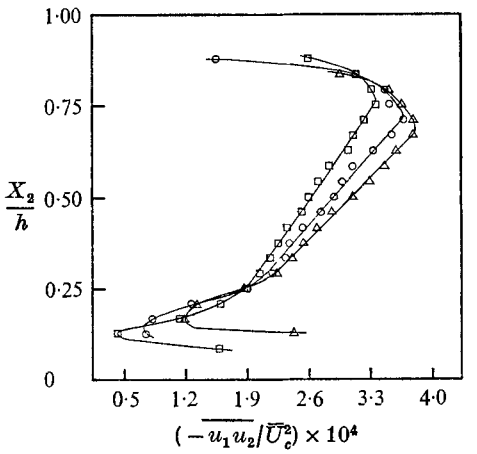

FIGURE 10. Lateral surveys of Reynolds stress with mean-velocity profile $\partial^2\overline{U}_1/\partial X_2^2 = 8{\cdot}4$ $(\text{ft s})^{-1}$, $X_3/h = -0{\cdot}07$. $\frac{3}{8}$ rods. Symbol key as for figure 3.

indication as to the sensitivity of the intensity distribution to the mean-velocity distribution.

Figure 9 presents the lateral surveys of the turbulence resulting from the velocity profile, generated with the $\frac{3}{8}$ rod grid, that has a constant negative mean-shear gradient. In this case, the fluctuating components vary linearly in the lateral direction, but with a slope that is opposite in sign to the flows with constant positive mean-shear gradients. The reason for this is the reversal of the lateral variation of total strain relative to the previous flows. In the present case, the the gradient $\partial u_1'/\partial X_2$ is negative, and its magnitude increases in the downstream direction.

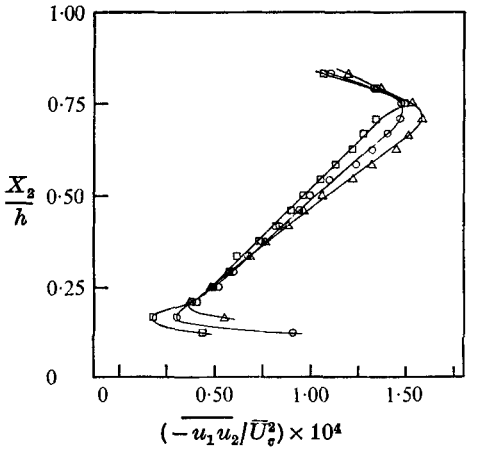

FIGURE 11. Lateral surveys of Reynolds stress with mean-velocity profile $\partial^2\overline{U}_1/\partial X^2 = 12{\cdot}3$ (ft s)$^{-1}$, $X_3/h = -0{\cdot}07$. $\frac{3}{16}$ rods. Symbol key as for figure 3.

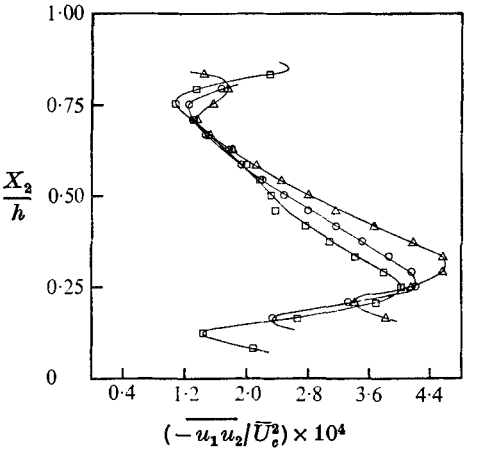

FIGURE 12. Lateral surveys of Reynolds stress with mean-velocity profile $\partial^2\overline{U}_1/\partial X_2^2 = -6{\cdot}7$ (ft s)$^{-1}$, $X_3/h = -0{\cdot}07$. $\frac{3}{8}$ rods. Symbol key as for figure 3.

Figures 10–12 show the lateral distributions of the turbulent shear stress non-dimensionalized by the square of the centre-line velocity $\overline{U}_c$. The first two cases are the result of the quadratic mean-velocity profiles with constant positive mean-shear gradients, the third case results from a quadratic mean-velocity profile with a constant negative mean-shear gradient. Figures 10 and 11 show that the turbulent shear stress varies linearly in the X_2 direction, and that the gradient $-\partial\overline{u_1u_2}/\partial X_2$ increases in the downstream direction. Figure 12 shows that the turbulent shear stress also varies linearly in the X_2 direction, but that the gradient $-\partial\overline{u_1u_2}/\partial X_2$ has the opposite sign, and therefore decreases in the downstream direction.

Since the mean shear $\partial\overline{U}_1/\partial X_2$ is positive in all portions of the flow fields not affected by the boundary layer, the quantity $\overline{u_1u_2}$ is negative at all points of interest. The Reynolds stress component, defined as $\tau_{12} = -\rho\overline{u_1u_2}$, is therefore positive without exception.

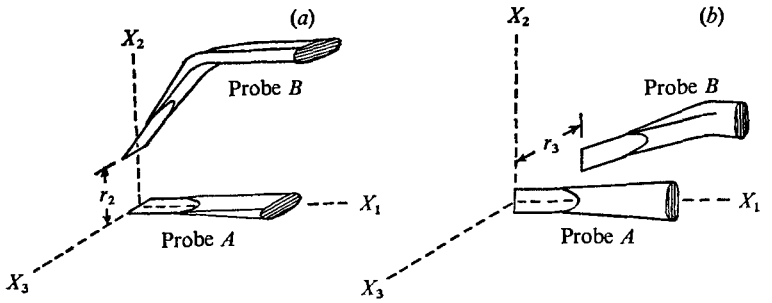

FIGURE 13. Measurement of two-point spatial velocity correlation coefficients: (*a*) $R_{11}(r_2)$; (*b*) $R_{11}(r_3)$.

3.4. *Two-point spatial velocity correlation coefficients*

The two-point spatial velocity correlation coefficient is defined as

$$R_{ij}(\mathbf{X},\mathbf{r}) = \frac{\overline{u_i(\mathbf{X})\,u_j(\mathbf{X}+\mathbf{r})}}{u_i'(\mathbf{X})\,u_j'(\mathbf{X}+\mathbf{r})}. \tag{1}$$

$u_i(\mathbf{X})$ is the fluctuating velocity in the i direction at a point in space identified by the vector $\mathbf{X}$, and $\mathbf{r}$ is the vector identifying the spatial separation of the two points. This expression reduces to

$$R_{11}(\mathbf{X},\mathbf{r}) = \frac{\overline{u_1(\mathbf{X})\,u_1(\mathbf{X}+\mathbf{r})}}{u_1'(\mathbf{X})\,u_1'(\mathbf{X}+\mathbf{r})} \tag{2}$$

for the measurements of this study. Recall that the u_1 fluctuating component is in the direction of the mean flow.

Data were taken at three longitudinal positions: $X_1/h = 5{\cdot}0$, $6{\cdot}7$ and $8{\cdot}5$ in the flows with constant positive mean-shear gradients. The use of these positions was dictated by external structural members of the wind tunnel. At each of these longitudinal positions, three lateral positions for data taking were chosen: $X_2/h = 0{\cdot}33$, $0{\cdot}50$ and $0{\cdot}67$. Spatial separations of the two single-wire probes were in either the X_2 or X_3 direction. Figure 13 shows the probe configurations used for taking measurements.

Figures 14 and 15 show that the correlation coefficient curves at a given longitudinal position are essentially identical at all three lateral positions. This holds true whether the separation is in the X_2 or X_3 direction. Figure 15 shows the greatest departure from this behaviour in the case of the $\frac{3}{16}$ rod generator with separation in the X_3 direction.

The correlation coefficients in the X_2 direction remain positive at all values of the separation. This phenomenon was observed by Rose (1966), Champagne *et al.* (1970) and others. Correlation coefficients with separation distances in the X_3 direction take on negative values as shown in figure 15. The incompressible mass conservation equation requires a negative transverse correlation coefficient at some positions in the plane normal to the mean flow so this negative region is to be expected.

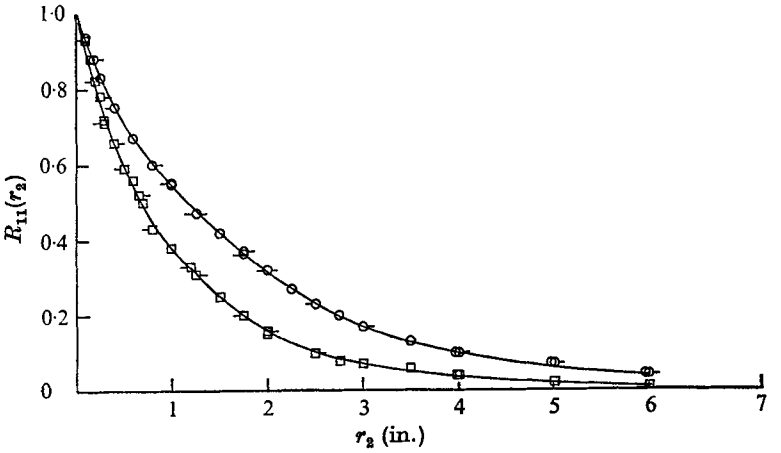

FIGURE 14. Two-point velocity correlation coefficient curves with separations in the X_2 direction. $X_1/h = 8{\cdot}5$.

X_2/h	$\frac{3}{8}$ rods	$\frac{3}{16}$ rods
0·33	-○	-□
0·50	○	□
0·67	○-	□-

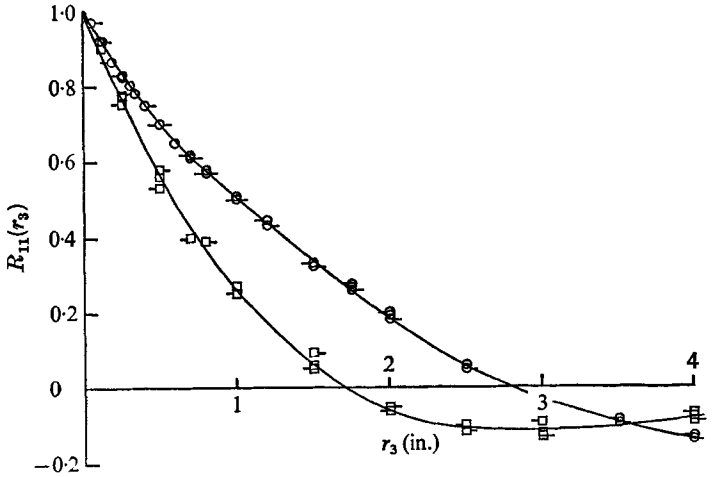

FIGURE 15. Two-point velocity correlation coefficient curves with separations in the X_3 direction. $X_1/h = 8{\cdot}5$. Symbol key as for figure 14.

Figures 16–19 show the downstream development of the $R_{11}(r_2)$ and $R_{11}(r_3)$ velocity correlation coefficients along the wind-tunnel centre-line for the same flows. The correlation coefficients increase in the downstream direction for any particular value of the two-point separation distance.

3.5. *Integral scales*

The longitudinal integral scale is defined as

$$L_1 = \int_0^\infty R_{11}(r_1, 0, 0)\, dr_1. \tag{3}$$

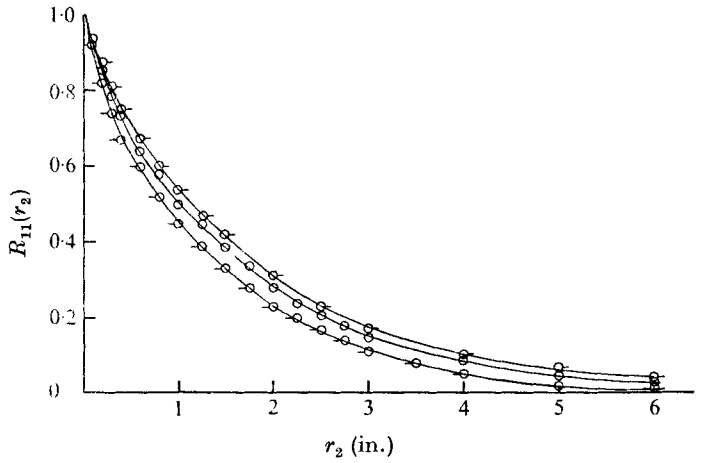

'IGURE 16. Longitudinal development of two-point correlation coefficient curves with separations in the X_2 direction. $\frac{3}{8}$ rods. $X_2/h = 0{\cdot}50$. X_1/h: -○, 5·0; ○, 6·7; ○-, 8.5.

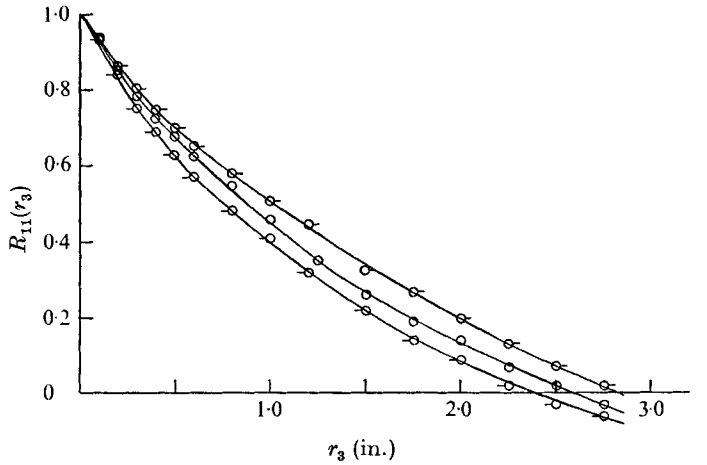

IGURE 17. Longitudinal development of two-point correlation coefficient curves with separations in the X_3 direction. $\frac{3}{8}$ rods. $X_2/h = 0{\cdot}50$. Symbol key as for figure 16.

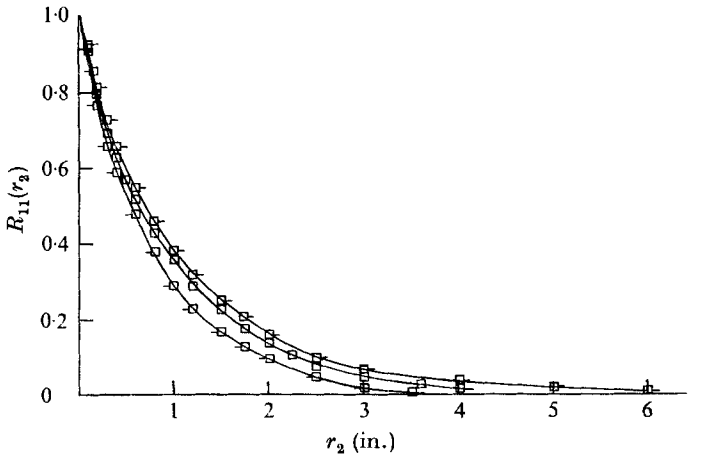

IGURE 18. Longitudinal development of two-point correlation coefficient curves with separations in the X_2 direction. $\frac{3}{16}$ rods. $X_2/h = 0{\cdot}50$. X_1/h: -□, 5·0; □, 6·7; □-, 8·5.

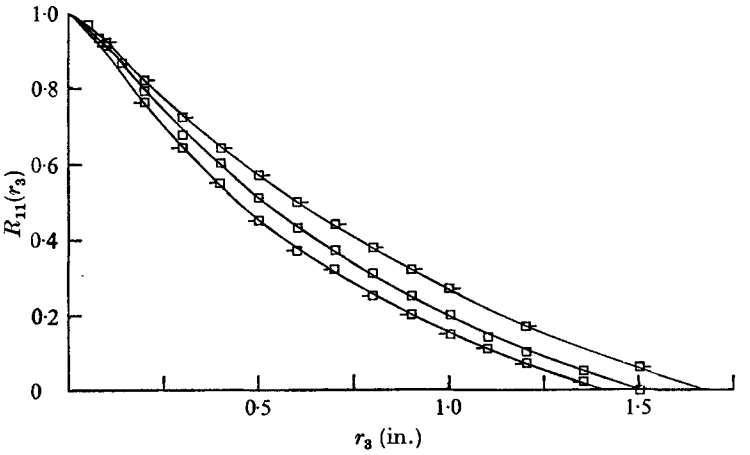

FIGURE 19. Longitudinal development of two-point correlation coefficient curves with separations in the X_3 direction. $\frac{3}{16}$ rods. $X_2/h = 0{\cdot}50$. Symbol key as for figure 18.

R_{11} is the two-point velocity correlation coefficient of the u_1 fluctuating compoment. Lateral integral scales L_2 and L_3 are defined in a similar manner, where the integrations, with respect to r_2 and r_3, are of $R_{11}(0, r_2, 0)$ and $R_{11}(0, 0, r_3)$. The integral scale characterizes the size of the energy-containing eddies in a turbulent flow. $R_{11}(r_1, 0, 0)$ is difficult to measure experimentally because of hot-wire interference effects. Consequently, the one-dimensional energy spectrum was used instead (Richards 1971).

The lateral integral scales require the measurement of the correlation coefficients to large distances (equation (3)). Owing to the limited size of the wind tunnel and the growth of the boundary layer, it was not always possible to separate the hot wires by a distance so large that the effective zero of the correlation coefficient function was reached. In the cases of $R_{11}(0, r_2, 0)$, the maximum separation distance used was eight inches, while in a few cases separation distances of about 3 in. were the maximum that could be attained. (This was especially a problem near the top and bottom, i.e. $x_2/h = 0{\cdot}33$ or $x_2/h = 0{\cdot}67$.) In these cases, the large-separation character of the correlation coefficient curves was approximated by exponential curves in a manner described by Rose (1966). In all cases, however, separations of at least three integral scales were possible.

The lateral correlation coefficient $R_{11}(0, 0, r_3)$ takes on negative values at relatively small values of r_3 (figures 17 and 19). These remain negative for the largest values of r_3 that can be achieved. Therefore, the first zero of the correlation coefficient function is used as the upper limit of integration to determine L_3.

Table 3 summarizes the values of the integral scales. The scales are relatively constant in the X_2 direction, even though the spacing of the rods in the generators is non-uniform. The rod spacing differs by 42% between $X_2/h = 0{\cdot}33$ and $X_2/h = 0{\cdot}67$, while the greatest lateral deviation in the value of an integral scale is $\pm 5\%$ from the mean. This occurs in the case of the $\frac{3}{16}$ rod grid for L_3.

Figure 20 shows the longitudinal development of the integral scales at the centre-line of the wind tunnel. As has been found in all previous investigations

X_1/h	5·0	6·7	8·5	8·5	8·5
X_2/h	0·5	0·5	0·5	0·33	0·67
$\frac{3}{8}$ rods					
L_1 (in.)†	2·18	2·71	3·48	—	—
L_2	1·34	1·55	1·73	1·71	1·69
L_3	0·90	1·02	1·16	1·15	1·12
X_1/h	5·0	6·7	8·5	8·5	8·5
X_2/h	0·5	0·5	0·5	0·33	0·67
$\frac{3}{16}$ rods					
L_1 (in.)†	1·32	1·46	1·80	—	—
L_2	0·83	1·00	1·11	1·08	1·11
L_3	0·54	0·60	0·69	0·66	0·73

TABLE 3. Summary of integral scales with mean velocity profile $\partial^2\overline{U}_1/\partial X_2^2 = 8{\cdot}4$ (ft s)$^{-1}$ or 12·3 (ft s)$^{-1}$. †Values determined from one-dimensional energy spectra.

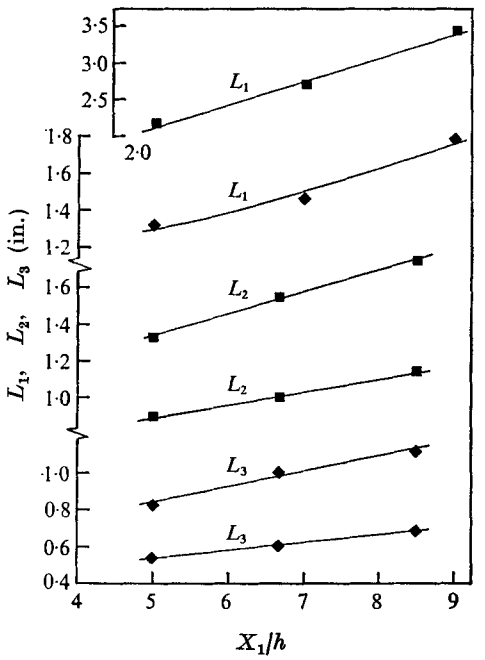

FIGURE 20. Longitudinal development of integral scales with mean-velocity profile $\partial^2\overline{U}_1/\partial X_2^2 = 8{\cdot}4$ (ft s)$^{-1}$, $X_2/h = 0{\cdot}50$, $X_3/h = -0{\cdot}07$. ■, $\frac{3}{8}$ rods; ◆, $\frac{3}{16}$ rods.

of turbulent shear flows with uniform mean shear, the integral scales increase monotonically in the flow direction.

One of the desired goals was to achieve a flow whose lateral extent was large compared with the integral scales. (Cf. § 1.) For the case of the $\frac{3}{8}$ grid (positive curvature), the worst case was $2L_2/H_e \simeq 0{\cdot}25$. For the $\frac{3}{16}$ grid, the worst case was 0·2. Here H_e is the lateral extent of the flow that was unaffected by the boundary layers. These numbers are so small that some confidence can be placed

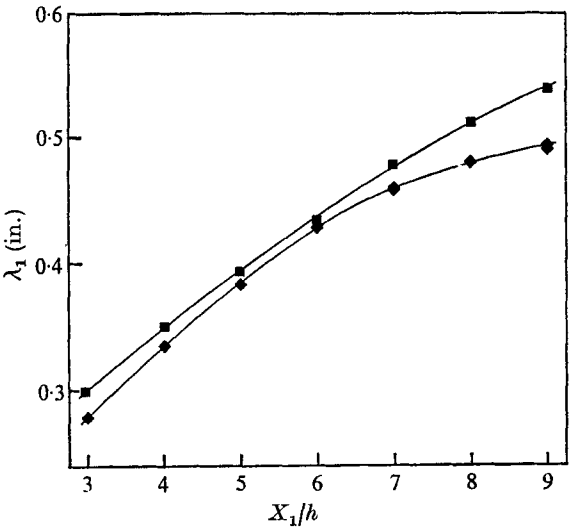

FIGURE 21. Longitudinal development of microscales with mean-velocity profile $\partial^2/\bar{U}_1/\partial X_2^2 = 8{\cdot}4$ (ft s)$^{-1}$, $X_2/h = 0{\cdot}50$, $X_3/h = -0{\cdot}07$. Symbol key as for figure 20.

in the results. These compare favourably with other investigations (e.g. the value of Champagne *et al.* for $2L_2/H_e \simeq 0{\cdot}24$). For the negative-curvature case, the field is somewhat narrower.

3.6. *Microscales*

The longitudinal Taylor microscale is defined by

$$\lambda_1^2 = \overline{2u_1^2}[\overline{(\partial u_1/\partial X_1)^2}]^{-1}. \tag{4}$$

The lateral Taylor microscales λ_2 and λ_3 are defined in the same manner, with the spatial derivatives in the X_2 and X_3 directions, respectively.† In addition, it is assumed that Taylor's hypothesis in the form

$$\partial/\partial t = -\bar{U}_1\,\partial/\partial X_1 \tag{5}$$

holds approximately for this flow field. The approximation identifies the temporal history at a fixed point with the convected spatial history; it has been found to hold in flows where the turbulence level is relatively small (Comte-Bellot & Corrsin 1971).

Combining equations (4) and (5) yields

$$\lambda_1^2 = 2\bar{U}_1^2\overline{u_1^2}[\overline{(\partial u_1/\partial t)^2}]^{-1}. \tag{6}$$

This allows one to determine the longitudinal microscale by differentiating the u_1 component of the turbulence with respect to time.

Figure 21 shows the longitudinal development of λ_1 along the centre-line of the wind tunnel. The λ_1 microscale of the turbulence is greater at any downstream position for the $\frac{3}{8}$ grid flow than for the $\frac{3}{16}$. For both test flows the microscale increases monotonically downstream, but the rate of increase decreases markedly for the $\frac{3}{16}$ rod grid at large values of X_1/h. A similar result is shown by Hwang

† This definition of λ_2^2 and λ_3^2 differs from that commonly used in isotropic turbulence by a factor of 2.

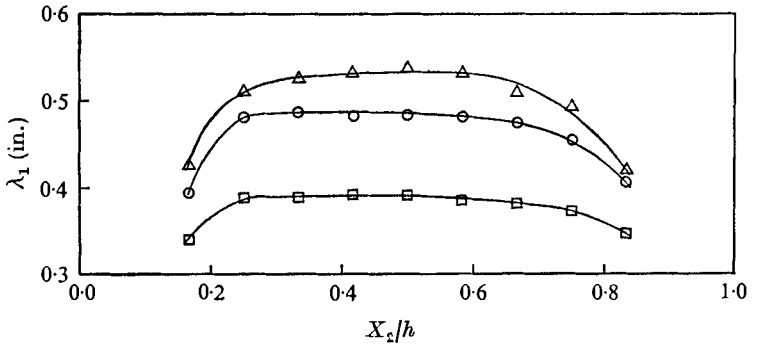

FIGURE 22. Lateral distributions of the microscale with mean-velocity profile $\partial^2\overline{U}_1/\partial X_2^2 = 8{\cdot}4\,(\text{ft s})^{-1}$, $X_3/h = -0{\cdot}07$. $\frac{3}{8}$ rods. Symbol key as for figure 3.

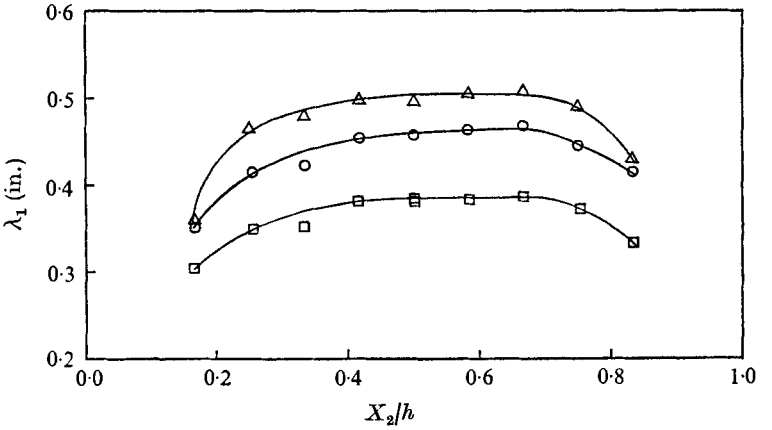

FIGURE 23. Lateral distributions of the microscale with mean-velocity profile $\partial^2\overline{U}_1/\partial X_2^2 = 12{\cdot}3\,(\text{ft s})^{-1}$, $X_3/h = -0{\cdot}07$. $\frac{3}{16}$ rods. Symbol key as for figure 3.

(1971). In his experiment, grid mesh-size is roughly analogous to rod spacing in the present experiment.

Figures 22 and 23 show the lateral distributions of the microscale λ_1 at various longitudinal positions. The microscale is more uniform laterally in the flow field generated by the $\frac{3}{8}$ rod grid than in that associated with the $\frac{3}{16}$ rods. Both figures show the microscales to be more laterally uniform than in the case reported by Rose (1966), where the flow field was also generated by a non-uniformly spaced round-rod grid.

The lateral microscales λ_2 and λ_3 must be evaluated in a different manner, since in these cases no simple approximation relating the spatial and temporal derivatives exists. In statistically-steady homogeneous turbulence it has been shown (Batchelor 1953) that, for vanishingly small values of the separation r_2, the two-point correlation coefficient $R_{11}(0, r_2, 0)$ can be approximated by the first two terms of a Taylor series, viz.

$$R_{11}(0, r_2, 0) \simeq 1 - r_2^2/\lambda_2^2. \tag{7}$$

This defines a parabola with vertex at $r_2 = 0$, $R_{11} = 1$, and provides a simple way

X_1/h	5·0	6·7	8·5	8·5	8·5
X_2/h	0·5	0·5	0·5	0·33	0·67
$\frac{3}{8}$ rod grid					
λ_1 (in.)	0·39	0·48	0·53	0·52	0·51
λ_2	0·34	0·37	0·37	0·37	0·37
λ_3	0·34	0·37	0·38	—	—
$\frac{3}{16}$ rod grid					
λ_1 (in.)	0·38	0·45	0·49	0·47	0·50
λ_2	0·32	0·33	0·32	0·32	0·32
λ_3	0·32	0·32	0·33	0·33	0·33

TABLE 4. Microscales in generated flow fields with mean-velocity profile $\partial^2\overline{U}_1/\partial X_2^2 = 8{\cdot}4$ (ft s)$^{-1}$ or 12·3 (ft s)$^{-1}$.

to evaluate λ_2 from the intersection of the parabola with the r_2 axis. The microscale λ_3 can be found in the same manner, where now

$$R_{11}(0,0,r_3) \simeq 1 - r_3^2/\lambda_3^2. \tag{8}$$

Rose (1966) suggested a method of finding the microscale graphically, by plotting the small separation data points against $(1-R_{11})$ on a log–log plot, then fitting a straight line with slope 2 to them. The intersection of the straight line with the ordinate value $(1-R_{11}) = 1$ establishes the value of the microscale. This method was used by Champagne *et al.* (1970) and Hwang (1971), as well as Rose (1966).

The results for the microscales are shown in table 4. We estimate that these values are accurate to $\pm 6\%$. From these data, it appears that λ_1 grows somewhat in the axial direction, but λ_2 and λ_3 do not, within the uncertainty of the measurements.

4. Analysis of experimental results

4.1. *Homogeneity and stationarity in the generated flow fields*

The experimental results of §3 demonstrated that the turbulence in this flow is not homogeneous in the X_1 and X_2 directions. That is to be expected, since the only possible mean-velocity profile to sustain a homogeneous turbulent field is linear. However, the degree the generated turbulent fields depart from homogeneity is of interest.

A criterion for homogeneity is that the mean flow and turbulence statistical properties vary by relatively small amounts over distances as large as the largest characteristic lengths of the turbulence. A mathematical statement of this criterion is given by Champagne *et al.* (1970) in the form

$$\Lambda/\overline{N}\,|\nabla\overline{N}| \ll 1. \tag{9}$$

$\overline{N}$ is a mean property, ∇ is the gradient operator, and Λ is the largest characteristic length of the turbulence (e.g. the integral scale L).

Figures 4–12, 20 and 21 show that inhomogeneities occur in the mean-square values of the turbulent velocity components, in the $\overline{u_1 u_2}$ shear-stress term in the

	$\frac{3}{8}$ rods	$\frac{3}{16}$ rods	Champagne *et al.* (1970)	Hwang (1971) $M = 2$
$(L_1/\lambda_1)\ (\partial\lambda_1/\partial X_1)$	0·0088	0·0028	0·015	0·0083
$(\partial L_1/\partial X_1)$	0·014	0·0048	0·010	0·014
$(L_1/u_1')\ (\partial u_1'/\partial X_1)$	0·0040	0·0026	—	—
$(L_1/u_3')\ (\partial u_3'/\partial X_1)$	0·0048	0·0025	—	—
$(L_1/\overline{u_1u_2})\ (\partial \overline{u_1u_2}/\partial X_1)$	0·00045	0·0027	—	—
$(L_2/u_1')\ (\partial u_1'/\partial X_2)$	0·041	0·042	—	—
$(L_2/u_2')\ (\partial u_2'/\partial X_2)$	0·035	0·037	—	—
$(L_2/\overline{u_1u_2})\ (\partial \overline{u_1u_2}/\partial X_2)$	0·070	0·079	—	—

TABLE 5. Departure from homogeneity of generated flow fields with mean velocity profile $\partial^2\overline{U}_1/\partial X_2^2 = 8{\cdot}4$ (ft s)$^{-1}$ or 12·3 (ft s)$^{-1}$. Wind-tunnel position: $X_1/h = 7{\cdot}0$, $X_2/h = 0{\cdot}50$, $X_3/h = -0{\cdot}07$.

X_1 and X_2 directions, and in the length scales L_1 and λ_1 in the X_1 direction. The results of calculations using (9) are given in table 5. In addition, table 5 includes results of Champagne *et al.* (1970) and Hwang (1971) for linear shear flows, and reveals that the values involving the gradients of the scales in the longitudinal direction are quite comparable. Departure from homogeneity in the X_1 direction of the fluctuating components is smaller than that of the scales, particularly in the case of the $\frac{3}{8}$ rod grid flow. It is concluded that, even though there is growth in the scales and fluctuating components, the rate is such that the flow is relatively homogeneous in the X_1 direction.

Applying the same criterion reveals that the turbulent quantities characterizing the flow field are much less homogeneous in the X_2 direction. The values obtained are an order of magnitude larger than comparable ones in the X_1 direction. This behaviour is totally unlike the results in linear shear flows, and must be attributed to the X_2 gradient in the mean shear.

As a test of stationarity in a frame of reference convected with the centre-line velocity $\overline{U}_c$, the characteristic length used previously is replaced by $T\overline{U}_c$. (T is the integral time scale in the convected frame.) Since T cannot be measured experimentally with the present instrumentation, it is measured following Champagne *et al.* (1970) as

$$\frac{1}{T} \simeq \frac{u_1'}{L_1} + \frac{\partial \overline{U}_1}{\partial X_2}. \tag{10}$$

$T \simeq 0{\cdot}045$ s for the $\frac{3}{8}$ rod grid flow and $T \simeq 0{\cdot}043$ for the $\frac{3}{16}$ case at $X_1/h = 7{\cdot}0$. The characteristic lengths $T\overline{U}_c$ are therefore approximately 2·3 and 2·2 ft, respectively. Substituting these values of $T\overline{U}_c$ in place of the integral scales L_1 in the relationships in table 3 yields values an order of magnitude larger than those previously obtained. Thus, with respect to the convected frame, the departure from homogeneity is greater in the longitudinal direction that that measured with respect to a fixed frame. It is roughly comparable with the homogeneity in the X_2 direction measured with respect to a fixed frame.

All results show that the turbulent field is in a state of continuing evolution.

X_1/h	α_σ (deg.), $\frac{3}{8}$ rods	α_σ (deg.), $\frac{3}{16}$ rods
5·0	−29, 61	−28, 62
7·0	−26, 64	−26, 64
9·0	−24, 66	−23, 67

TABLE 6. Principal axes of turbulent stresses with mean velocity profile $\partial^2\overline{U}_1/\partial X^2 = 8{\cdot}4$ (ft s)$^{-1}$ or 12·3 (ft s)$^{-1}$. Wind-tunnel position: $X_2/h = 0{\cdot}50$, $X_3/h = -0{\cdot}07$.

X_1/h	σ_a/σ_b $\frac{3}{8}$ rods	σ_a/σ_b $\frac{3}{16}$ rods
5·0	2·7	3·0
7·0	3·4	3·7
9·0	3·5	3·4

TABLE 7. Ratios of principal turbulent stresses in the X_1, X_2 plane with mean velocity profile $\partial^2\overline{U}_1/\partial X_2^2 = 8{\cdot}4$ (ft s)$^{-1}$ or 12·3 (ft s)$^{-1}$. Wind-tunnel position: $X_2/h = 0{\cdot}50$, $X_3/h = -0{\cdot}07$.

4.2. *Axes of principal turbulent stresses*

The principal axes of the turbulent stresses in the X_1, X_2 plane for rectilinear two-dimensional mean flows are given by

$$\alpha_\sigma = \tfrac{1}{2}\tan^{-1} 2\overline{u_1 u_2}[\overline{u_1^2} - \overline{u_2^2}]^{-1}. \tag{11}$$

α_σ is the angle between the direction of the mean flow and the principal axes of the turbulent shear stress. Using data presented in figures 7, 8, 10 and 11, and equation (11), the orientations of the principal axes for the flows with constant positive mean-shear gradients have been computed at several downstream positions; they are presented in table 6. These results show that the principal axes of the mean stresses, which are at $\pm 45°$ for this flow, and the principal axes of the turbulent stresses are not aligned. Further, they show that the turbulent stress principal axes and the mean-flow principal axes diverge as the flow proceeds in the X_1 direction. This was observed by Hwang (1971) in a linear shear flow for that part of it in which the turbulence was still decaying. The values of α_σ at $X_1/h = 5{\cdot}0$ in this experiment (−29, 61; −28, 62°) are similar to those obtained by Champagne *et al.* (1970) (−28, 62°) in the 'nearly' homogeneous part of their flow field.

The magnitudes of the principal stresses in the X_1, X_2 plane are given by

$$-\sigma_{a,b} = \tfrac{1}{2}(\overline{u_1^2} + \overline{u_2^2}) \pm [\tfrac{1}{2}(\overline{u_1^2} - \overline{u_2^2})^2 + (\overline{u_1 u_2})^2]^{\frac{1}{2}}. \tag{12}$$

The ratios of these magnitudes are calculated at the same tunnel positions as in table 6. The results of these calculations are presented in table 7. It is of interest that the magnitude of the ratio σ_a/σ_b for the flow at $X_1/h = 5{\cdot}0$ is roughly the same as that found by Hwang (1971) in the approximately homogeneous part of his flow.

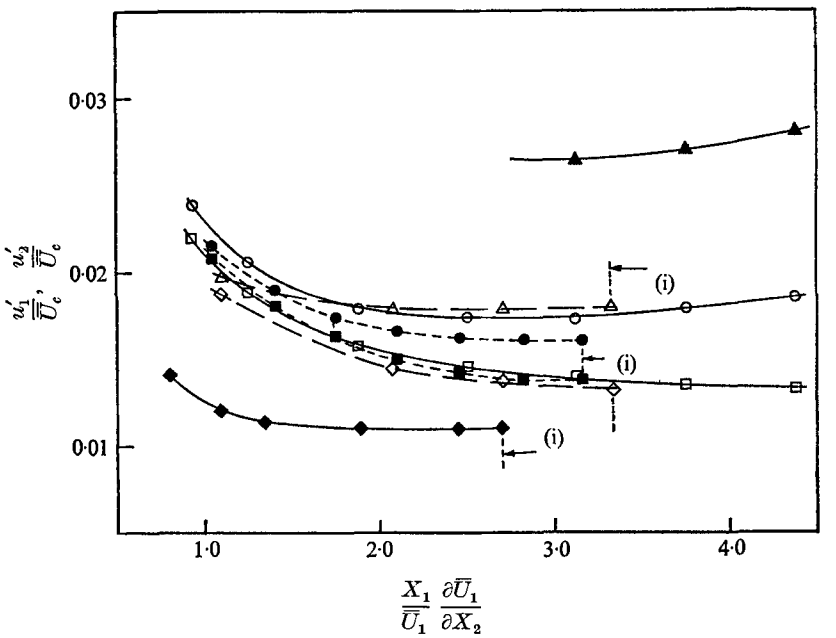

FIGURE 24 Longitudinal development of turbulence against total strain $(X_1/\overline{U}_1)(\partial\overline{U}_1/\partial X_2)$. (i) Exit plane. (Richards 1971, linear mean profile.)

	$\frac{3}{16}$ rods	Hwang (1971) 2 in. mesh	Champagne *et al.* (1970)	Richards (1971) $\frac{3}{8}$ rods	Rose (1966)
$u_1'/\overline{U}_c$	○	●	△	▲	◆
$u_2'/\overline{U}_c$	□	■	◇		

4.3. *Gradient of turbulent component energies in the longitudinal direction*

A particular feature of the results of this investigation is the growth of the energy in the u_1 and u_3 components, after they reach minimum values at about $X_1/h = 5{\cdot}0$ on the tunnel centre-line, for all profiles. Growth in the u_2 component energy is also evident, but smaller. This behaviour was observed in investigations using linear mean-velocity profiles, provided the total strain was sufficiently large.

Recent theoretical papers by Lumley (1965), Townsend (1970) and Deissler (1970) stressed that equilibrium states are not reached in a developing turbulent shear flow. The results of this investigation tend to support these theoretical ideas.

Computed values of the total strain $(X_1/\overline{U}_1)(\partial\overline{U}_1/\partial X_2)$ are presented in table 8 for all three test flows. Centre-line values at $X_1/h = 9{\cdot}0$ are about the same in all cases: viz. 5·6. Except for Harris *et al.*, previous linear mean profile investigations yielded values of the strains considerably lower than this.

In the cases presented by Rose (1966), Champagne *et al.* (1970) and Hwang (1971), the centre-line exit plane strains were 2·7, 3·3 and 3·2, respectively. Thus, it appears likely that the growth of the turbulent component energies was not observed because the turbulence did not undergo sufficiently large total strain. Figure 24 supports this supposition. It is a plot of selected data from several

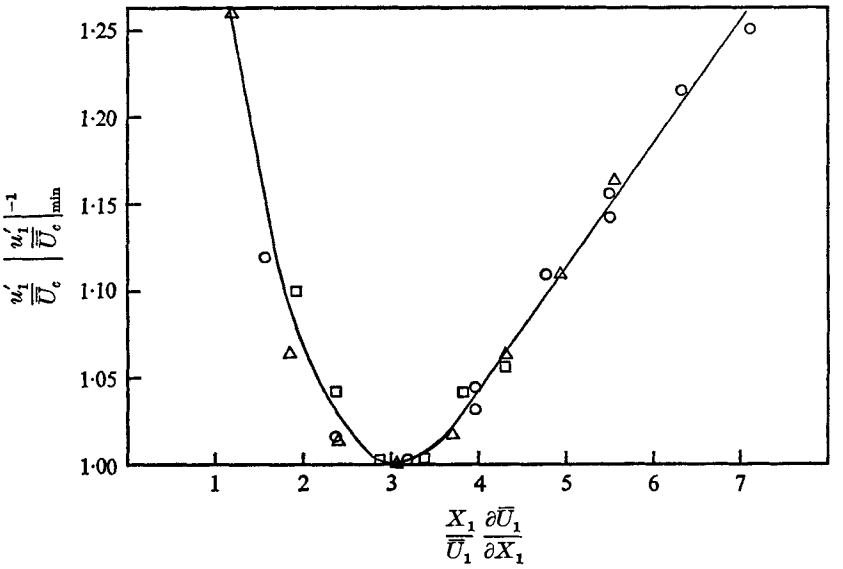

FIGURE 25. Longitudinal development of turbulence against total strain $(X_1/\overline{U}_1)\times(\partial\overline{U}_1/\partial X_2)$ with mean-velocity profile $\partial^2\overline{U}_1/\partial X_2^2 = -6{\cdot}7$ (ft s)$^{-1}$, $X_3/h = -0{\cdot}07$. $\frac{3}{8}$ rods. X_2/h: ○, 0·33; △, 0·50; □, 0·67.

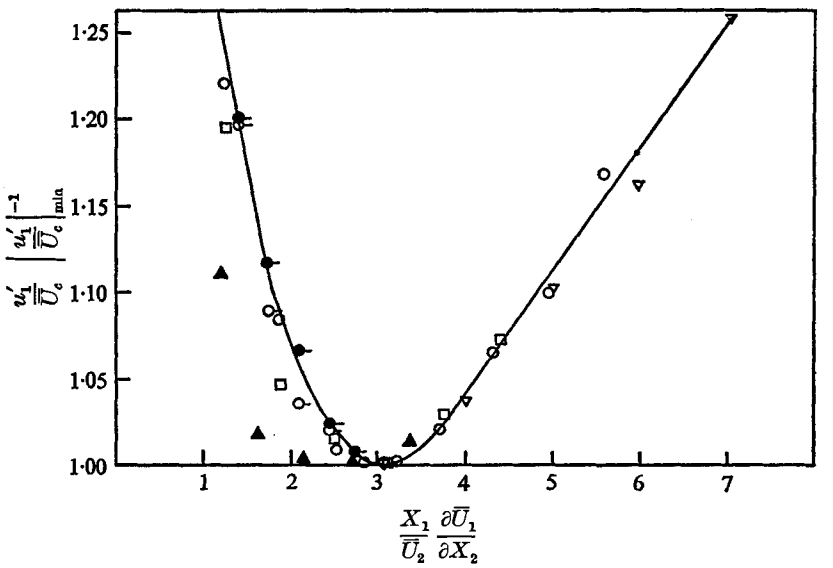

FIGURE 26. Longitudinal development of turbulence against total strain $(X_1/\overline{U}_1)\times(\partial\overline{U}_1/\partial X_2)$. ●–, Hwang (1971), $\frac{1}{2}$ in. mesh; ○–, Hwang (1971), 2 in. mesh; ○, $\frac{3}{8}$ rods, linear profile (Richards 1971); □, $\frac{3}{16}$ rods, $\partial^2\overline{U}_1/\partial X_2^2 = 12{\cdot}3$ (ft s)$^{-1}$; ——, $\frac{3}{8}$ rods, $\partial^2\overline{U}_1/\partial X_2^2 = -6{\cdot}7$ (ft s)$^{-1}$; ▲, Champagne *et al.* (1970); ▽, Harris *et al.*

X_1/h	X_2/h	$\frac{3}{8}$ rods $\frac{\partial^2\overline{U}_1}{\partial X_2^2} = 8{\cdot}4$ (ft s)$^{-1}$	$\frac{3}{8}$ rods $\frac{\partial^2\overline{U}_1}{\partial X_2^2} = -6{\cdot}7$ (ft s)$^{-1}$	$\frac{3}{16}$ rods $\frac{\partial^2\overline{U}_1}{\partial X_2^2} = 12{\cdot}3$ (ft s)$^{-1}$
5·0	0·33	2·81	3·97	2·52
	0·50	3·10	3·08	3·12
	0·67	3·29	2·39	3·52
7·0	0·33	3·94	5·56	3·53
	0·50	4·35	4·32	4·37
	0·67	4·61	3·34	4·93
9·0	0·33	5·06	7·15	4·54
	0·50	5·59	5·55	5·62
	0·67	5·92	4·30	6·34

TABLE 8. Total mean strain $(X_1/\overline{U}_1)\,(\partial\overline{U}_1/\partial X_2)$ at various positions. $X_3/h = -0{\cdot}07$.

experiments that had similar turbulent energy levels, excepting Rose (1966) and the linear mean-velocity flow of Richards (1971).

The development in the present work is quite similar to that in Champagne *et al.* (1970) and Hwang (1971). The growth phase of the u_1 component energy is just being reached in the first two cases, if it is to occur. The plot of the data with a linear mean velocity profile from Richards (1971) shows clearly the increase in the u_1 component energy.

The results of Rose (1966), while at a somewhat lower turbulence level, reflect constant values of u_1' for a variation of total strain from 1·8 to 2·7. The results of Champagne *et al.* (1970), as plotted in figure 24, show a similar behaviour, viz. $u_1' \simeq$ constant for the range $1{\cdot}9 \leqslant (X_1/\overline{U}_1)\,(\partial\overline{U}_1/\partial X_2) \leqslant 3{\cdot}3$. The results of this study show that u_1' varies by less than 3% in the range of total strain $2{\cdot}0 \leqslant (X_1/\overline{U}_1)\,(\partial\overline{U}_1/\partial X_2) \leqslant 3{\cdot}6$; thus the results in that particular range of total strain are not dissimilar from those of Champagne *et al.*

Figure 25 further reinforces the notion that the longitudinal development of the turbulence is dependent primarily upon the total strain. This plot was obtained from data gathered from a single flow at three different lateral positions normalized by the minimum value of the ratio $u_1'/\overline{U}_1$ at each lateral position. It shows clearly that a strain of about 3·0 is where the minimum value of the fluctuating u_1' component is reached regardless of lateral position. The minimum value of u_1' reached in each case of course depends on the mean shear to which the turbulence has been subjected and the initial level of turbulence introduced by the grid. Figure 26 compares the results of various other test flows with the composite curve of figure 25.

Figures 4–6 confirm that, for the flows studied in this investigation, the u_1' and u_3' component energies reach minima at total strains of about 3·0, and the u_2' component energy reaches its minimum at a total strain of about 4·5. This value for the u_1' component minimum is about the same as that reported by Rose (1970) and Hwang (1971) at the position where their turbulence reaches its minimum level in linear shear flows produced with three-dimensional generators.

The authors would like to thank Dr W. G. Rose for his helpful suggestions during this investigation.

REFERENCES

BATCHELOR, G. K. 1953 *The Theory of Homogeneous Turbulence.* Cambridge University Press.

CHAMPAGNE, F. H., HARRIS, V. G. & CORRSIN, S. 1970 Experiments on nearly homogeneous turbulent shear flow. *J. Fluid Mech.* **41**, 81.

COMTE-BELLOT, G. & CORRSIN, S. 1971 Simple Eulerian time correlation of full- and narrow-band velocity signals in grid-generated, 'isotropic' turbulence. *J. Fluid Mech.* **48**, 273.

CORRSIN, S. 1957 *Proc. 1st Naval Hydro. Symp., Nat. Acad. Sci./Nat. Res. Coun. Publ.* no. 515, p. 373.

DEISSLER, R. G. 1970 Effect of initial condition on weak homogeneous turbulence with uniform shear. *Phys. Fluids*, **13**, 1868.

HINZE, J. O. 1959 *Turbulence.* McGraw-Hill.

HWANG, W. S. 1971 Experimental investigation of turbulent shear flows. Ph.D. dissertation, Department of Aerospace Engineering and Engineering Physics, University of Virginia.

LUMLEY, J. L. 1965 Interpretation of time spectra measured in high-intensity shear flows. *Phys. Fluids*, **8**, 1056.

RICHARDS, H. K. 1971 Experimental investigation of turbulent shear flow with quadratic mean velocity profiles. Ph.D. thesis, University of Virginia.

ROSE, W. G. 1966 Results of an attempt to generate a homogeneous turbulent shear flow. *J. Fluid Mech.* **44**, 767.

ROSE, W. G. 1970 Interaction of grid turbulence with a uniform mean shear. *J. Fluid Mech.* **44**, 767.

TOWNSEND, A. A. 1970 Entrainment and the structure of turbulent flow. *J. Fluid Mech.* **41**, 13.